

Effects of Heating and Quenching Processing Parameters on Phase Transformation of 55CrMo Steel

Haijuan Liu, Huiping Li, Zhichao Li, and Lianfang He

(Submitted June 11, 2017; in revised form May 17, 2018; published online September 13, 2018)

Microstructure and mechanical properties after induction hardening have a significant effect on the wear resistance performance and lifetime of 55CrMo steel ball screw. In the paper, the dilatometric curves were recorded at the different heating rate by a Gleeble-1500D thermo-mechanical simulator to determine the effect of heating rate on the austenitizing temperature of 55CrMo steel. Heat treatment of some specimens was performed by the Gleeble-1500D thermal simulator at the different heating temperature, holding time and cooling rate to investigate the effect of induction hardening parameters on the phase transformation, microstructure and microhardness of 55CrMo steel. Microstructure of specimen was analyzed using an optical microscope and a scanning electron microscope. Volume fraction of retained austenite was measured using an x-ray diffractometer. The mechanical properties were evaluated by a microhardness tester. The results show that the austenitizing temperature of 55CrMo steel increases with the increasing heating rate. Increasing the heating temperature, holding time and cooling rate of specimen is helpful in obtaining a uniform cryptocrystalline martensite. Volume fraction of retained austenite is less as the heating temperature is in the range of 900-950 °C. In the induction hardening of 55CrMo steel, the heating temperature should be in the range of 900-1000 °C.

Keywords dilatometric curve, microstructure, phase transformation, rapid heating

1. Introduction

The precision ball screw is an important functional part in CNC (Computerized Numerical Control) machine tools, and its failure forms are generally wear and fatigue. Under certain conditions, hardness is directly related to the wear resistance of material (Ref 1). As a method to improve the strength and hardness of metals, martensite transformation is a more effective way, and hardness has become an important indicator to assess the wear resistance of the workpiece in many industries (Ref 2). At present, increasing the surface hardness of ball screw by induction hardening is the main method to improve the wear resistance of ball screw and prolong the lifetime of ball screw (Ref 3). However, it is prone to produce the non-uniform surface hardness, poor wear resistance or other problems during the induction hardening of ball screw. These problems severely hinder the development of CNC machine tools and manufacturing equipment (Ref 4). In order to attain the optimum processing parameters of heat treatment, several studies have been carried out to investigate the mechanical properties and phase transformation in the induction hardening (Ref 5-7).

Kim et al. (Ref 8) studied the effects of induction hardening and tempering on the mechanical properties of medium-carbon SPS5 steel. Kristoffersen et al. (Ref 9) reported that the process parameters of induction hardening affect the residual stress state

of the quenched parts. Revilla et al. (Ref 10) analyzed the effects of different heating rates on low-alloy carbon steel and found that high heating rates combined with short holding times help to refine the carbide size and increase the hardness. Zhu et al. (Ref 11) studied the effects of induction heating rate on the performance of Ni/Al phase. Danon et al. (Ref 12) studied the effects of heating rate on the austenitization start temperature A_{c1} , end temperature A_{c3} , austenite-transformation time, and rate of austenitization.

In addition, some scholars carried out the numerical simulation of induction hardening (Ref 13-15). Using the numerical simulation results, the heating temperature distribution and phase transformation could be predicted by establishing the model, thus better optimizing the induction heating parameters. Li et al. (Ref 16) used the finite element method (FEM) for the simulation of stress-strain field in the quenching, and a finite element simulation software was developed for evaluating the stress/strain fields in the quenched parts. Yuan et al. (Ref 17) developed a FEM modeling to determine the key parameters in the induction hardening, especially for determining phase transformation and hardness. Zhang et al. (Ref 18) simulated the induction hardening of S45 axis by a commercial FEM software ANSYS and proposed a method for determining the induction heating parameters. To improve the uniformity of the hardened layer, Hömberg (Ref 19) and Barglik (Ref 20) studied dual-frequency induction hardening, and the PDELIB and FLUX 3D software were used to simulate the process. According to the simulation results, many induction hardening technologies were developed to improve the uniformity of hardened layer for mechanical parts.

The structure obtained after the induction heating and quenching depends on the heating conditions, such as the heating temperature, cooling rate, composition of steel, and original structure. During the heat treatment, the unevenness of austenitization component caused by the heterogeneity of austenitization temperature in the induction hardening of ball

Haijuan Liu, Huiping Li, Zhichao Li, and Lianfang He, School of Materials Science and Engineering, Shandong University of Science and Technology, Qingdao 266510 Shandong, China. Contact e-mail: lihuiping99@163.com.

screw increased the unevenness of the hardness, residual stress, and deformation (Ref 21). In addition, the heterogeneity of the initial austenite affected the type of phase transformation (Ref 22). The initial microstructure and heating rate affected the microstructural development for the induction heat treatment of 5150 steel (Ref 23). For all the aforementioned reasons, it is necessary to study the phase transformation characteristics of materials during the induction hardening and select the optimal useful performance.

For 5010-type ball screw of 55CrMo steel, the heating rate of the surface layer is approximately 50 °C/s when it is heated using a double induction coils with a gap of 30 mm between the coils (Ref 24). Under the conditions of rapid heating, austenitization of steel during the heating and phase transformation characteristics of microstructure during the cooling are different from those of conventional heat treatment processes (Ref 25). Induction heating exclusively relies on phase transformation to enhance the surface wear resistance and fatigue resistance. However, only a small number of study results have been published regarding austenitization during the rapid heating and phase transformation during the cooling.

To investigate the effects of processing parameters such as heating temperature, holding time and cooling rate on the phase transformation temperature, microstructure and mechanical properties of 55CrMo steel, dilatometry is one of the more useful techniques. Phase transformation causes volume changes, which can be recorded by studying the length changes in samples with normalized dimensions during heating or cooling, and the relationship between expansion and temperature can be obtained by the thermal expansion experiments (Ref 26). According to the induction heating and cooling rates of ball screw, the specimens of 55CrMo steel were first heated at different temperatures at the heating rate of 50 °C/s, and then cooled at the different rates using a Gleeble-1500D thermo-mechanical simulator. Microstructure of specimen was analyzed using an optical microscope and a scanning electron microscope. Volume fraction of retained austenite was mea-

sured using an x-ray diffractometer. The mechanical properties were evaluated by a microhardness tester.

2. Experiment

A medium-carbon alloy 55CrMo steel produced by a company is used in this study. The initial microstructure is ferrite + pearlite, as shown in Fig. 1. The chemical composition of 55CrMo steel measured using an optical emission spectrometer ARL-3460 is shown in Table 1 (Ref 21).

Some specimens of 55CrMo steel with the sizes of $\Phi 6 \times 10$ mm were machined using a wire electric discharge machine (WEDM). In order to determine the effect of the heating rates on the dilatometric curves of 55CrMo steel, according to the standard YB/T 5128-93 (determination of continuous cooling transformation diagram—dilatometric method), the specimens of 55CrMo steel were, respectively, heated up to 950 °C at the heating rates of 0.05, 0.3, 1.0, 5.0 and 50 °C/s by the Gleeble-1500D thermo-mechanical simulator. According to the dilatometric curves, the austenitization temperatures can be obtained using the tangent method at different heating rates.

In the reference (Ref 24), the induction hardening of 55CrMo steel ball screw is simulated using finite element method. The temperature curves of ball screw show that the heating rate for the material in the surface region is approximately 50 °C/s, the holding time can be changed in the range of 8-32 s by changing the moving speed of coils or changing the gap between the coils and the spraying water circle. In order to study the effect of heating temperature, holding time and cooling rate on the microstructure and microhardness of 55CrMo steel, the Gleeble-1500D thermo-mechanical simulator was used to control the heating and cooling process of the specimens, and record the dilatometric curves. The specimens of 55CrMo steel were first heated up to 800, 850, 900, 950, 1000, 1100 or 1200 °C at the heating rate of 50 °C/s, kept the temperature for 8, 16, or 32 s, and then cooled at the rate of 50, 70 or 90 °C/s. The experiment condition testing the dilatometric curves is shown in Fig. 2.

During the testing, the temperature in the middle of the specimen was tested using a thermocouple. According to the temperature from the feedback, the heating temperature, heating rate, and cooling rate can be controlled. The expansion of the specimens during the heating and cooling was recorded using a strain gauge. The dilatometric curves were measured, and then the austenitization temperature of 55CrMo steel was analyzed by the tangent method.

Because of the non-uniformity of temperature at the heated specimens, the position of the thermocouple and strain gauges was located in the middle section, and the specimens after testing were cut into two parts along the middle section using the WEDM. The specimens were prepared, sectioned, ground and polished. Then, the final microstructures were observed after the surfaces were etched with 4% nitric acid and alcohol solution. Metallographic characterization was performed by

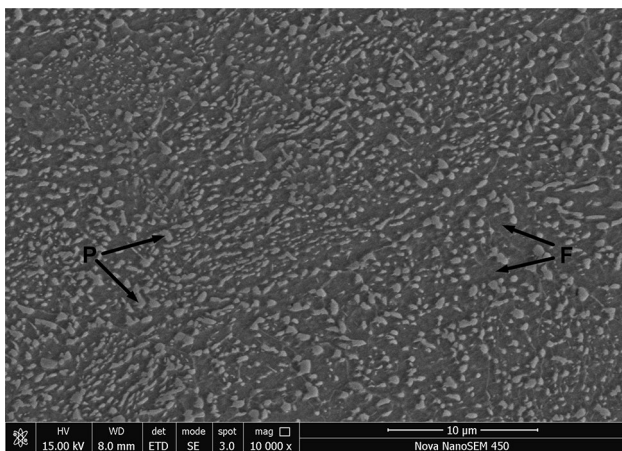


Fig. 1 Original microstructure of 55CrMo steel (recorded using the SE mode of Nova SEM 450)

Table 1 Chemical composition of 55CrMo steel (wt.%)

C	Si	Mn	P	S	Cr	Mo	Ni	Cu	V
0.58	0.24	0.89	0.015	0.002	0.89	0.22	0.017	0.015	0.004

optical microscope (Nikon ME600). The phase ratio of microstructure was roughly calculated using the Image Pro software of a metallographic microscope (ZEISS Axio Lab A1). In addition, electron microstructure analysis was carried out using a high-resolution scanning electron microscope (FEI Nova Nano SEM450). The mechanical properties were evaluated by a Vickers microhardness indenter (FM-700/SVDM4R) with an applied load of 200 gf for a loading time of 10 s according to the UNE-EN ISO 6507-1 standard. Microstructure and hardness of specimens are used to better interpret the slope changes in the dilatometric curves.

The retained austenite was characterized using an x-ray diffractometer (D/Max 2500PC) and Cu-K α radiation, operating at 100 mA, 40 kV, and a step of 0.02 $^\circ$ with the step-scanning method. The volume fraction of retained austenite was determined using the direct comparison method, involving the use of integrated intensities of (200) $_\gamma$, (220) $_\gamma$, and (311) $_\gamma$ with (200) $_\alpha$ and (211) $_\alpha$ peaks. The volume fraction of retained austenite V_A is calculated using Eq 1 (Ref 27):

$$V_A = \frac{1.4I_\gamma}{I_\alpha + 1.4I_\gamma} \quad (\text{Eq 1})$$

where I_γ is the integrated intensity of austenite and I_α is the integrated intensity of α -phase.

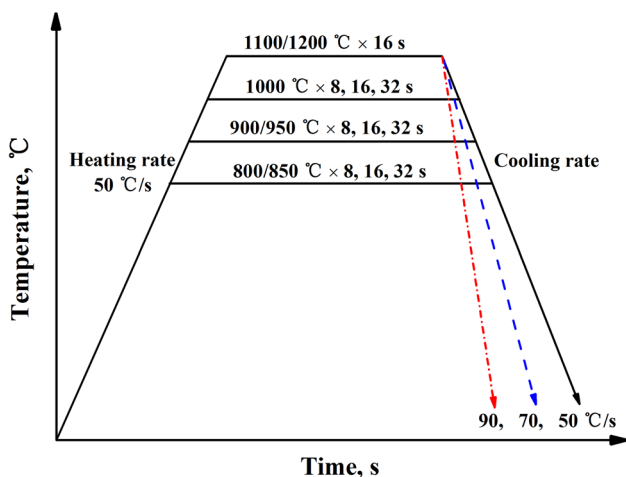


Fig. 2 Experiment condition testing the dilatometric curves

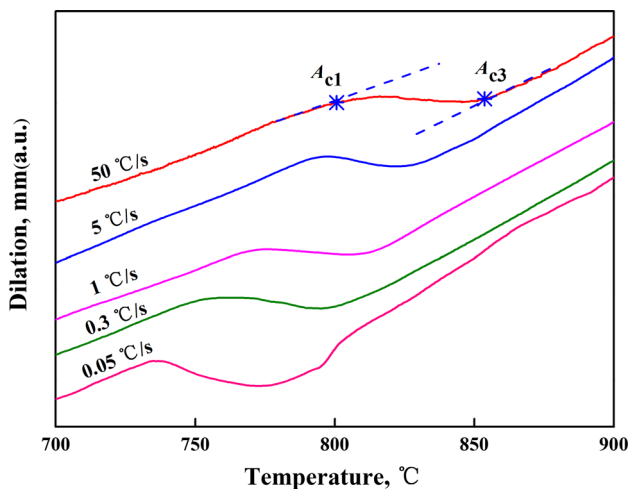
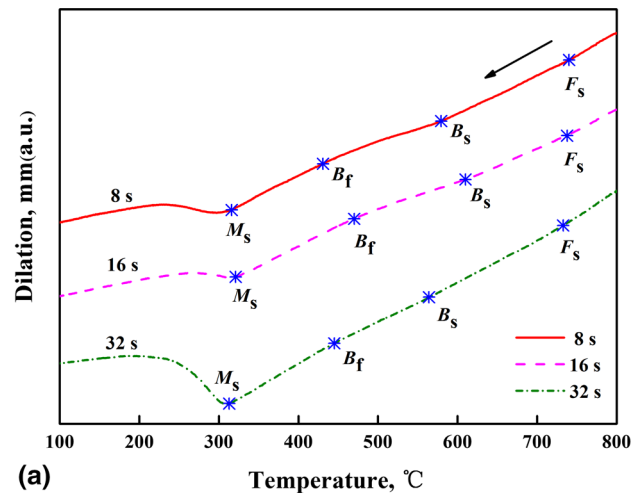
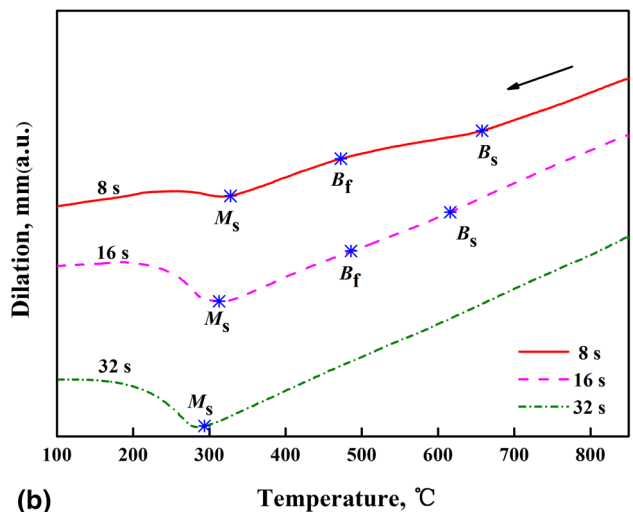


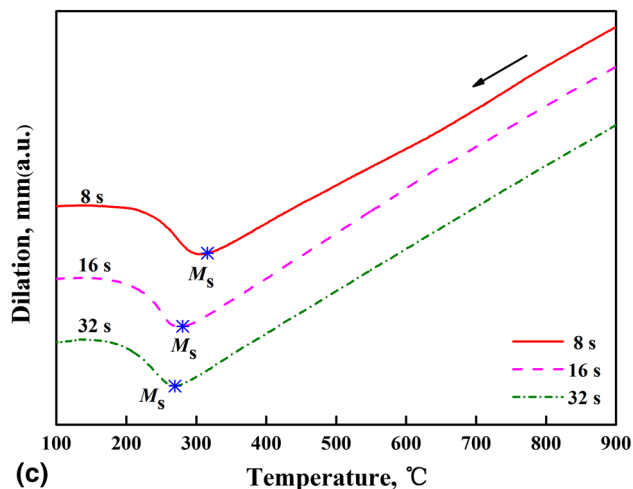
Fig. 3 Dilatometric curves of 55CrMo steel at the different heating rates



(a) Temperature, $^\circ\text{C}$



(b) Temperature, $^\circ\text{C}$



(c) Temperature, $^\circ\text{C}$

Fig. 4 Dilatometric curves of 55CrMo steel for the different holding times: (a) 800 $^\circ\text{C}$, (b) 850 $^\circ\text{C}$, (c) 900 $^\circ\text{C}$

3. Results and Discussion

3.1 Determination of Austenitization Temperature

The tangent method (Ref 28, 29) was used to analyze the dilatometric curve recorded at the different heating rates, and estimate the start and end temperatures of phase transformation,

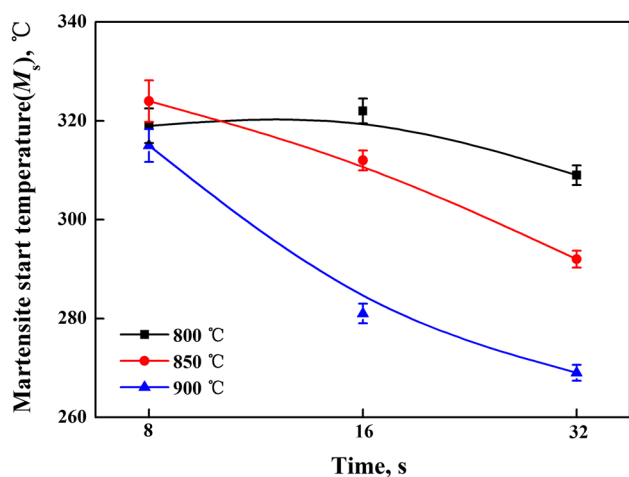


Fig. 5 Relationship between holding time and M_s ,

as shown in Fig. 3. When the heating rate is 0.05, 0.3, 1.0, 5.0 and 50 °C/s, the start temperatures of austenite formation (A_{c1}) are approximately 736, 752, 769, 793 and 802 °C, while the end temperatures (A_{c3}) are approximately 779, 796, 814, 830 and 854 °C, respectively. The heating rate has a significant effect on the austenitization temperatures A_{c1} and A_{c3} of 55CrMo steel. In the austenitizing process of 55CrMo steel, the rapid heating can increase the austenitization temperature, and temperatures A_{c1} and A_{c3} increase with the increasing heating rate. According to the results in the reference (Ref 24), the following experiments were conducted at the heating rate of 50 °C/s.

3.2 Effect of Holding Time on Phase Transformation of 55CrMo Steel

As the heating temperature is 800, 850 or 900 °C, and the holding time is 8, 16 or 32 s, the dilatometric curves recorded by the Gleeble-1500D thermal simulator at the cooling rate of 50 °C/s are shown in Fig. 4.

As the heating temperature is 800 °C, three turning points can be observed in the dilatometric curves in the temperature range of 400-800 °C. During the cooling, a few austenite is transformed into ferrite and pearlite in the high-temperature stage, some austenite is transformed into bainite in the mid-temperature stage, and the other austenite is transformed into martensite in the low-temperature stage. When the heating temperature is 800 °C, the ferrite + pearlite, bainite, and

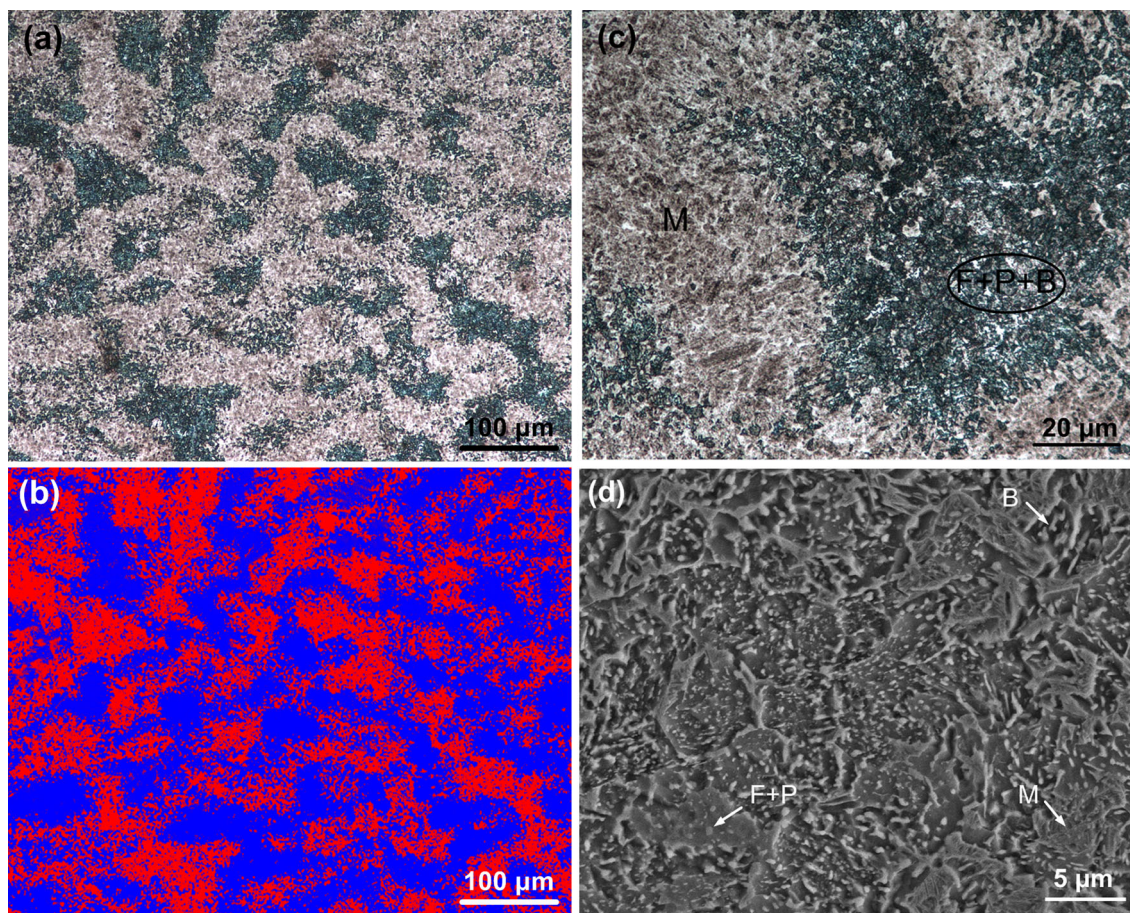


Fig. 6 Microstructure of 55CrMo steel heated at 800 °C for 8 s. (a) Low-magnification metallographic photograph, (b) Phase ratio diagram attained by the phase ratio analysis software, (c) High-magnification metallographic photograph, (d) SEM micrograph

martensite transformations are produced in the cooling process. According to the changes in the dilatometric curves, the volume fraction of bainite gradually decreases, whereas the volume fraction of martensite gradually increases.

As the heating temperature is 850 °C, bainite and martensite transformations are produced in the cooling process of specimen heated for 8 and 16 s at 850 °C. With the increasing holding time, the temperature range of bainite transition becomes narrow. The austenite formed in the heating process is completely transformed into martensite in the cooling process of specimen heated for 32 s at 850 °C.

As the heating temperature is 900 °C, there is no obvious turning point in the dilatometric curves in the temperature range of 400–800 °C. This shows that the initial pearlite can fully transform into austenite in the heating process.

For the different heating temperature and holding time, the relationship between the holding time and the martensite start temperature (M_s) is shown in Fig. 5. With the increasing holding time, M_s temperature decreases. The reason is that a longer holding time is helpful for the further integration of carbon and alloying elements into the austenite.

With the increasing heating rate, the start and end temperatures of austenitization move to a higher temperature due to the high heating rate. The dilatometric curves in Fig. 3 show that as the heating temperature is 800 °C, the heating temperature is less than the temperature A_{c1} (802 °C), ferrite + pearlite in the microstructure of specimen cannot be transformed into austenite in the heating process, but ferrite + pearlite in the microstructure of specimen is partly transformed into austenite in the stage of holding time. Ferrite cannot be completely transformed into austenite due to the low heating temperature

Table 2 Proportions of microstructure for the different holding times

Content, %	800 °C			850 °C		
	8 s	16 s	32 s	8 s	16 s	32 s
Ferrite + pearlite	10.13%	8.26%	4.41%	6.2%	0	0
Bainite	31.32%	27.64%	12.39%	30.4%	14.8%	0
Martensite	58.55%	64.1%	83.2%	63.4%	85.2%	100%

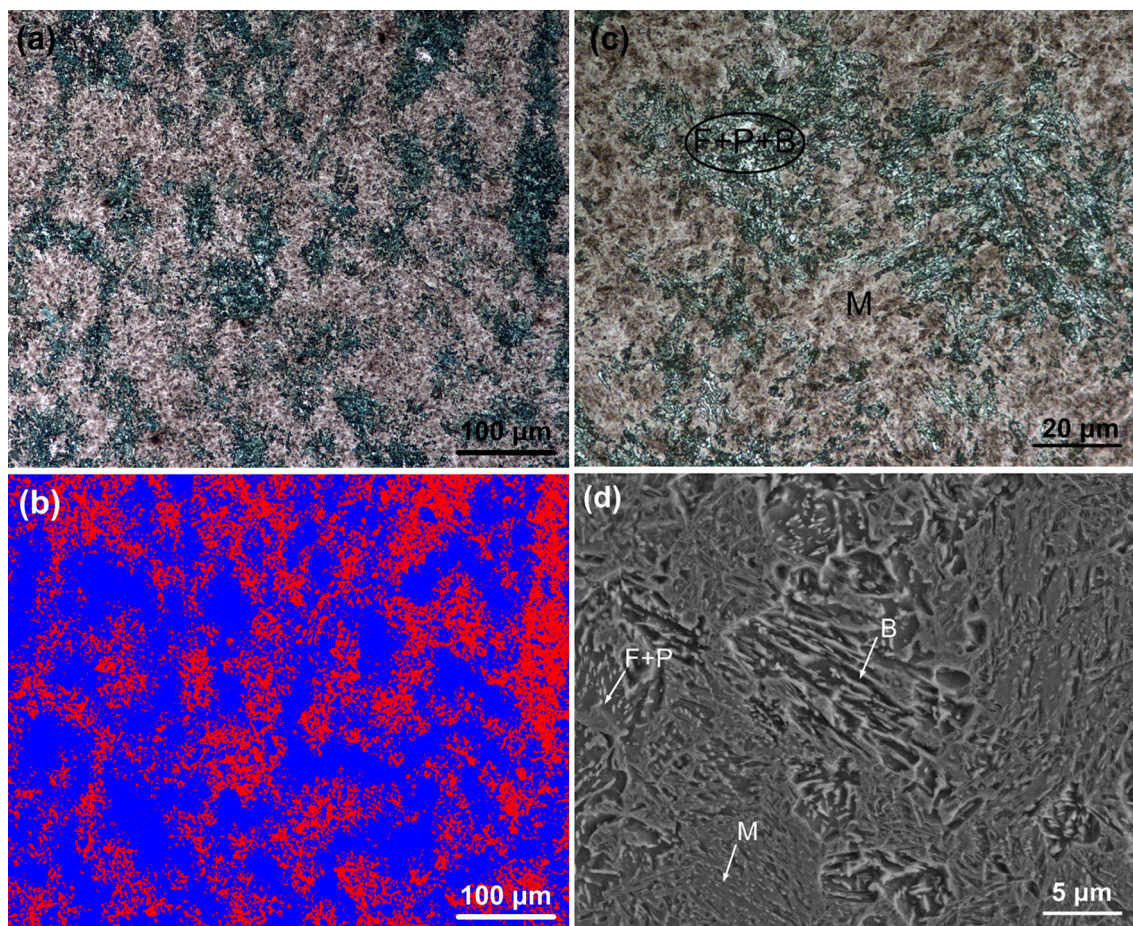


Fig. 7 Microstructure of 55CrMo steel heated at 800 °C for 16 s. (a) Low-magnification metallographic photograph, (b) Phase ratio diagram attained by the phase ratio analysis software, (c) High-magnification metallographic photograph, (d) SEM micrograph

and the short holding time. In addition, the ferrite transformation is produced at the high-temperature stage during the cooling. This is because the new ferrite grows from the retained ferrite without the development of an interface and the cooling rate is not large enough (Ref 30). The retained ferrite provides an explanation for new ferrite, shifting the ferrite transformation curve to the left. Moreover, bainite nucleation is mainly controlled by the diffusion of carbon atoms and nucleation occurs in the carbon-poor austenite region (Ref 31). Both the amount of carbon and alloying elements in the austenite matrix are reduced as the austenitizing treatment is incomplete (Ref 22). Hence, the bainitic transformation can be produced. In turn, it is helpful for the diffusion of carbon atoms and nucleation of austenite to increase the heating temperature and holding time. With the increasing heating temperature and holding time, the volume fraction of ferrite + pearlite transformed to austenite increases, the total carbon content in austenite can be increased. Thus, the volume fraction of bainite transformation reduces, and the volume fraction of martensitic transformation increases.

As the heating temperature is 800 °C, the holding time is 8 s and the cooling rate is 50 °C/s, the low-magnification metallographic photograph of microstructure is shown in Fig. 6(a), the high-magnification metallographic photograph of microstructure is shown in Fig. 6(c). The dark green regions represent ferrite + pearlite and bainite, which are not uniform. The dark gray regions represent martensite, which is cryptocrystalline martensite. Even though the fine cryptocrystalline

martensite is produced in the cooling process, a large amount of a mixture of ferrite + pearlite and bainite is also produced. The microstructure in Fig. 6(a) is well consistent with the results obtained according to the dilatometric curves in Fig. 4(a). The phase ratio analysis software of a metallographic microscope (ZEISS Axio Lab A1) can be used to estimate the volume fraction of different phases. The phase ratio diagram attained by the phase ratio analysis software is shown in Fig. 6(b). The volume fraction of diffusional phase transformation (ferrite + pearlite, bainite) and non-diffusional phase transformation (martensite) can be calculated according to the areas of different regions. The phases due to the diffusional phase transformation have the similar morphologies and fine-scale structure, it is impossible to distinguish the bainite and pearlite in the metallographic photograph of microstructure. SEM micrographs with the better resolution can be used to distinguish the bainite and pearlite. To identify the microstructure in the dark green regions with certainty, SEM micrographs were used to estimate the proportion of bainite and pearlite, as shown in Fig. 6(d). As the holding time is 8 s, the proportion of each phase is shown in Table 2.

As the holding time is 16 and 32 s, the low-magnification metallographic photograph of microstructure is shown in Fig. 7(a) and 8(a), the high-magnification metallographic photograph of microstructure is shown in Fig. 7(c) and 8(c), the phase ratio diagram attained by the phase ratio analysis software is shown in Fig. 7(b) and 8(b), SEM micrographs are used to estimate the proportion of bainite and pearlite is shown

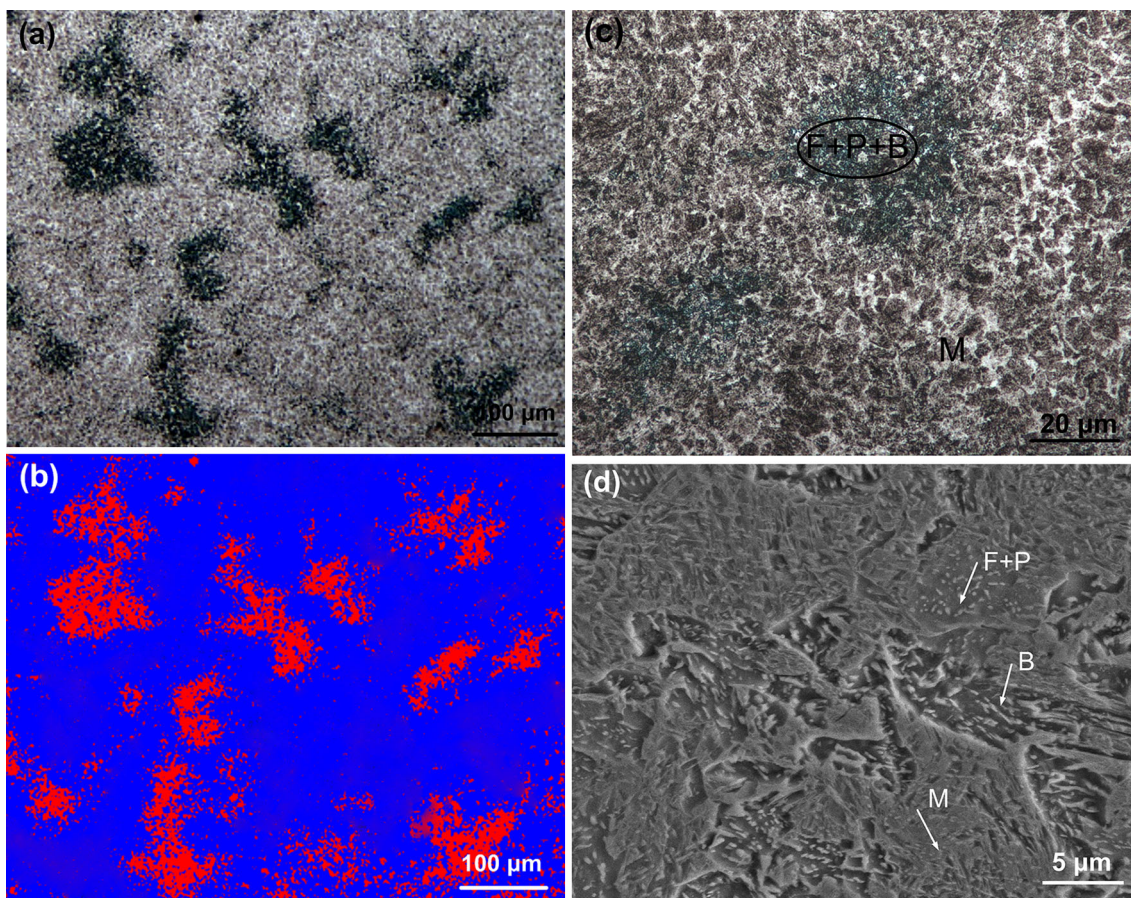


Fig. 8 Microstructure of 55CrMo steel heated at 800 °C for 32 s. (a) Low-magnification metallographic photograph, (b) Phase ratio diagram attained by the phase ratio analysis software, (c) High-magnification metallographic photograph, (d) SEM micrograph

in Fig. 7(d) and 8(d). Using the same method, the proportion of ferrite + pearlite and bainite can be estimated from the metallographic photograph and SEM image. The proportion of each phase is shown in Table 2.

Figure 6, 7 and 8 and the data in Table 2 show that microstructure of specimen is depending on the holding time. With the increasing holding time, the volume fraction of ferrite + pearlite and bainite decreases, and the volume fraction of martensite increases. Most of martensite structure is fuzzy and difficult to distinguish, indicating that the quenching temperature is low and it is not a normal microstructure.

The microhardness of specimen heated at 800 °C and 850 °C is shown in Fig. 9. It shows that the hardness of specimen fluctuates significantly from 200 HV to 700 HV as the heating temperature is 800 °C. The mechanical properties are not uniform and poor. The hardness variation of specimen can be explained by their respective microstructural constituents. With the increase in the holding time, the hardness variation reduces and the hardness increases. The reason is that the volume fraction of diffusional phase transformation with low hardness reduces with the increasing holding time, as shown in Fig. 6, 7 and 8. As the heating temperature is 850 °C and the holding time is 8 s, the hardness of specimen fluctuates significantly, but the hardness of specimen fluctuates slightly as the holding time is 16 or 32 s. Therefore, for the induction

hardening of 55CrMo steel, the heating temperature should be not less than 850 °C to attain much more martensite with high hardness and improve the uniformity of hardness.

As the heating temperature is 850 °C, the holding time is 8 s and the cooling rate is 50 °C/s, the low-magnification metallographic photograph of microstructure is shown in Fig. 10(a), the high-magnification metallographic photograph of microstructure is shown in Fig. 10(c). The phase ratio diagram attained by the phase ratio analysis software is shown in Fig. 10(b). SEM micrographs are used to estimate the proportion of bainite and pearlite is shown in Fig. 10(d). The microstructure consists of ferrite + pearlite, bainite and cryptocrystalline martensite. The dark green regions represent ferrite + pearlite and bainite, which are not uniform. The dark gray regions represent the cryptocrystalline martensite surrounded by a light-colored boundary, which is high-carbon martensite.

As the heating temperature is 850 °C and the holding time is 16 s, the low-magnification metallographic photograph of microstructure is shown in Fig. 11(a), the high-magnification metallographic photograph of microstructure is shown in Fig. 11(c). The phase ratio diagram attained by the phase ratio analysis software is shown in Fig. 11(b). SEM micrographs are used to estimate the proportion of bainite and pearlite is shown in Fig. 11(d). Some bainite can be found in the microstructure but no ferrite + pearlite. It is well consistent with the results obtained according to the dilatometric curves in Fig. 4(b). Using the same method, the proportion of each phase can be estimated, as shown in Table 2.

As the heating temperature is 850 °C and the holding time is 32 s, the low-magnification metallographic photograph of microstructure is shown in Fig. 12(a), and SEM micrographs are shown in Fig. 12(b). It is basically a complete martensite microstructure, and difficult to find bainite and ferrite + pearlite in the microstructure. With the increasing holding time, the residual carbides are decomposed, and the carbon content in austenite increases, the degree of homogenization increases, the continuous cooling transformation curve (Ref 21) shifts to the right, the bainite content gradually decreases. Compared to the metallographic photograph shown in Fig. 11, the content of white lumpy structure in Fig. 12(a) is much more than that in Fig. 11(a). It means that the volume fraction of high-carbon cryptocrystalline martensite increases. The increasing holding time is beneficial to the diffusion and homogenization of carbon. Thus, the amount of carbon dissolved in the austenite increases, and the amount of carbon in the martensite increases, finally it results in the increasing proportion of high-carbon cryptocrystalline martensite. Figure 9(b) shows that with the increasing holding time, the hardness of the sample increases, and the uniformity of hardness is significantly improved. Except increasing the heating temperature during the induction heating, prolonging the holding time also can promote the homogenization of carbon and alloying elements inside the austenite, thus suppressing the aggregation of carbon elements to form cementite, decreasing the rate of nucleation of cementite, inhibiting bainite transformation, promoting martensite formation (Ref 32).

The bainite microstructures consist of both the granular bainite (GB) and ferrite bainite (FB) phases, and the morphology was clearly observed in the SEM image as shown in Fig. 13. Owing to the lack of cooling, bainite is easily corroded into black, as observed using an optical microscope for the large black group, and the surface of the image observed by the

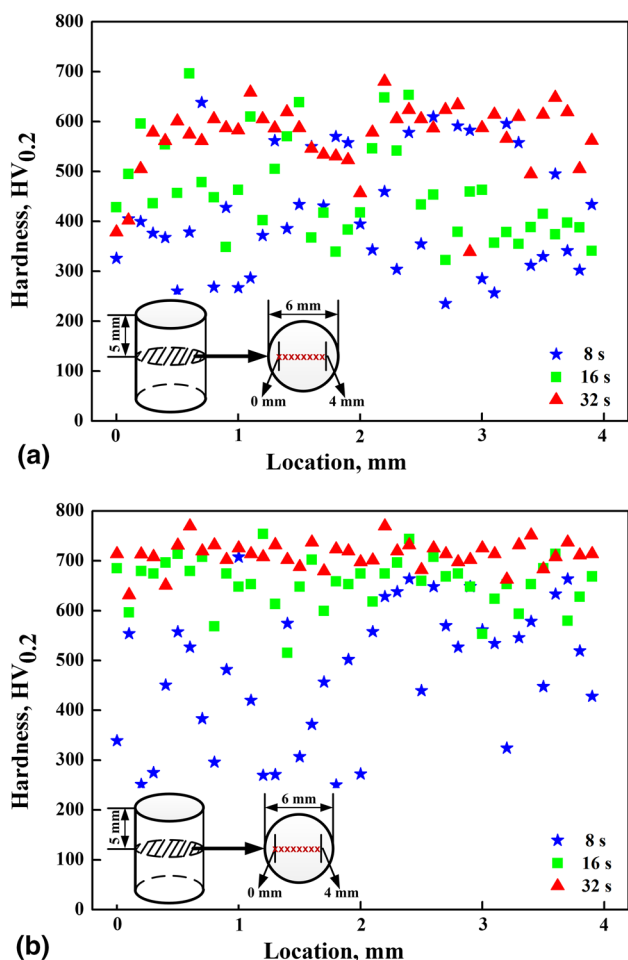


Fig. 9 Microhardness distribution of 55CrMo steel for different holding times. (a) Heated at 800 °C, (b) Heated at 850 °C

scanning electron microscope has a strong three-dimensional sense. This is derived from the stabilization of the austenite-stabilized region of the alloying element. A further discrimination feature for bainite is its morphology. To reveal this in detail, typical TEM micrographs of bainite were observed by Zaefferer (Ref 33). The nucleation of FB is heterogeneous, usually located in the austenite grain boundary. The FB grows along the grain boundary or into the crystal. The FB generally shows lamellar morphologies. The GB morphology shows a relatively coarse ferrite block with some cementite particles and isolated islands. Similar structures have been observed by Zhang (Ref 34), and they interpreted the structure as “granular bainite.” The island-like morphology is very irregular, and the structure of these isolated islands was not clearly observed using an optical microscope.

The distribution of carbon and alloying elements in the austenite was uneven in the microarea (Ref 35). The original high-carbon pearlite region was transformed into a high-carbon cryptocrystalline martensite with a white and smaller region. The low-carbon ferrite region was transformed into a darker crystalline martensite + bainite. In the bright area of general network distribution, the carbide at the austenite grain boundary first dissolves. Therefore, the contents of carbon and alloying elements are more than the crystal. Thus, the M_s points toward lower, and the martensite formed during the cooling is not prone to self-tempering. Therefore, martensite is not susceptible

to erosion, and it was gray. However, the carbide present in the austenite crystal dissolves less, and there are no dissolved carbide particles. Carbon and alloying elements melt less into austenite, and the M_s points toward higher. The martensite was prone to self-tempering during the cooling, and it was gray-black after erosion. With the increasing heating temperature and holding time, the light regions increase, and the dark regions decrease accordingly.

Under the rapid heating condition, the initial grain of the austenite becomes thinner, and it is difficult to grow. The degree of superheat in the steel becomes very large, resulting in an increase in the driving force $\Delta G_{\alpha \rightarrow \gamma}$ for phase transformation and nucleation (Ref 36). This increases the number of nucleation sites in austenite, refines the austenite grain, and inhibits the grain growth. The martensitic transformation is produced under the rapid cooling, and the microstructure is changed into a fine martensite structure. On the other hand, under the rapid heating condition, the non-uniform carbon distribution in the austenite region increases. Thus, the size of the microarea with a similar carbon content in the austenite decreases, and the difference in the martensitic formation temperature M_s points of each microregion clearly increases. This limits the shear rate of the hardened martensite, making the martensite crystals difficult to grow and refine, and ultimately forming fine cryptocrystalline martensite after the final quenching.

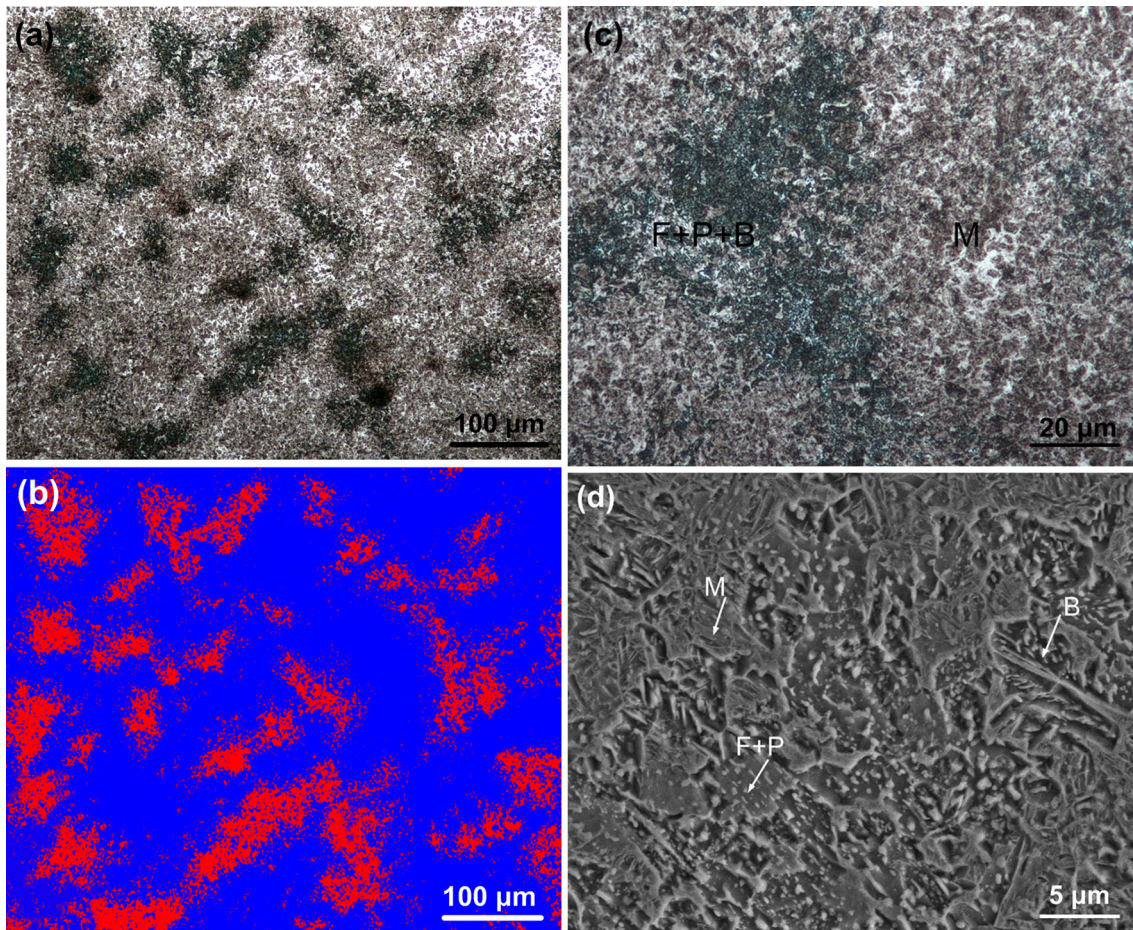


Fig. 10 Microstructure of 55CrMo steel heated at 850 °C for 8 s. (a) Low-magnification metallographic photograph, (b) Phase ratio diagram attained by the phase ratio analysis software, (c) High-magnification metallographic photograph, (d) SEM micrograph

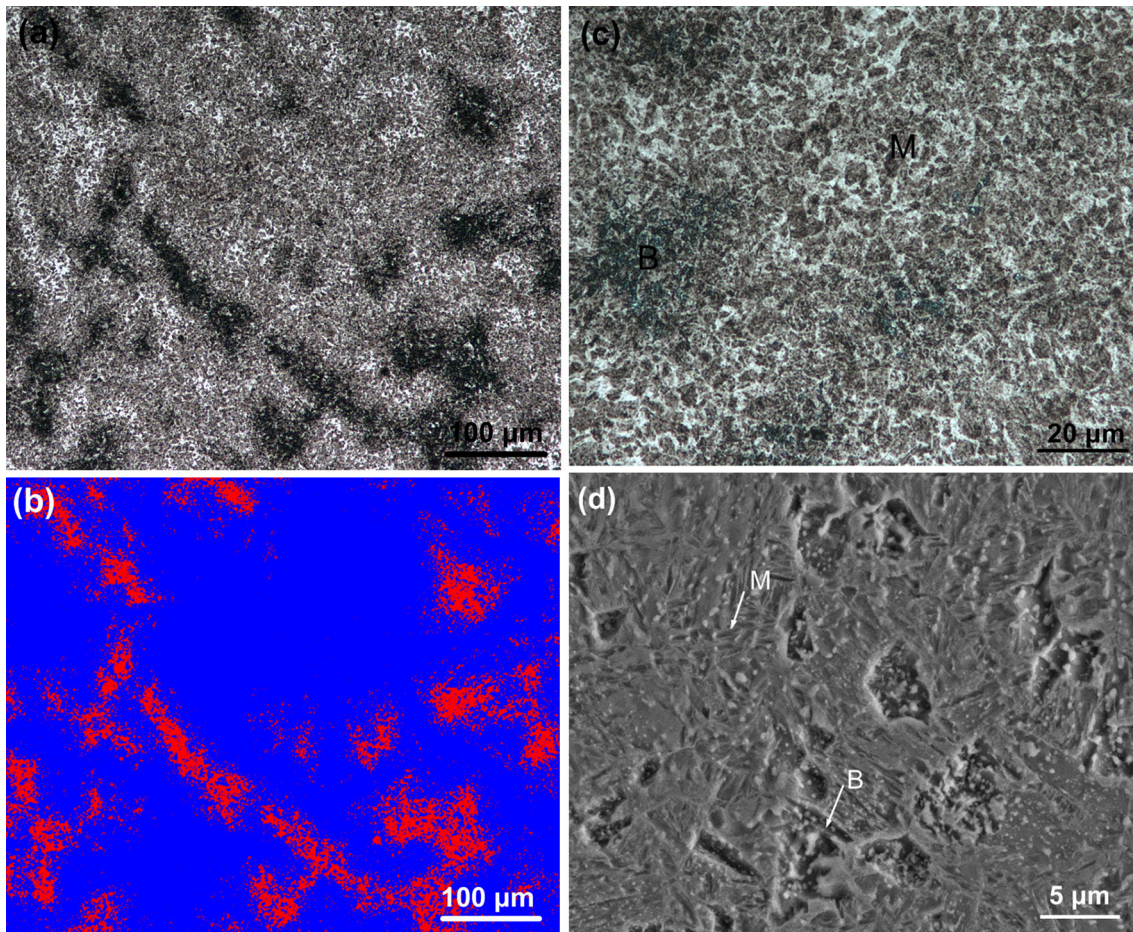


Fig. 11 Microstructure of 55CrMo steel heated at 850 °C for 16 s. (a) Low-magnification metallographic photograph, (b) Phase ratio diagram attained by the phase ratio analysis software, (c) High-magnification metallographic photograph, (d) SEM micrograph

Therefore, two temperature–time paths of 800 °C–(8, 16, and 32 s) and 850 °C–(8 and 16 s) were selected to account for the effect of an incomplete austenitization treatments and an incomplete austenitization on accelerating the bainite phase transformation (Ref 22). When the heating temperature is 900 °C, the optical metallographic photograph of microstructure is shown in Fig. 14. The microstructure is basically uniform for cryptocrystalline martensite. In addition, the selected XRD pattern is shown in Fig. 15. By calculating the volume fraction of retained austenite of 55CrMo steel specimen heated at 900 °C for the different holding times (Fig. 16), it shows that the volume fraction of retained austenite decreases with the increasing holding time. This is because the average alloying element content in the austenite is uniform and decreases with the increasing holding time, thus decreasing the volume fraction of retained austenite at room temperature. The mean hardness of 55CrMo steel specimen heated at 800 °C, 850 °C and 900 °C for the different holding time is shown in Fig. 17. With the increasing holding time, the hardness shows an increasing trend. Furthermore, the higher the temperature, the longer the time, and the higher the hardness.

3.3 Effect of Cooling Rate on Phase Transformation of 55CrMo Steel

The cooling rate significantly affected the phase transformation. During the cooling, the phase transformation types can

be better determined according to the dilatometric curves. The dilatometric curves of 55CrMo steel samples heated at the different heating temperatures for 16 s and cooled at the different cooling rates are shown in Fig. 18. According to the dilatometric curves depending on the heating temperatures and cooling rates, the phase transformation types and temperature can be determined using the tangent method, as shown in Fig. 18. The start and end temperatures of bainite formation are B_s and B_f , respectively. Martensite starting temperature is M_s .

The phase transformations during the cooling occurred at the different temperatures are depending on the cooling rates. As the heating temperature is 800 and 850 °C, the phases attained at the cooling rate of 50 and 70 °C/s are the mixture of bainite and martensite, but only martensite transformation appears at the cooling rate of 90 °C/s. In this regard, the volume fraction of bainite in the mixed microstructure decreases with the increasing the cooling rates. The fast cooling rate can inhibit the ferrite and bainite transformations. The different cooling rates result in the different phase types and volume fraction of the phases. Thus, increasing the cooling rate can cause the continuous cooling transformation curve to shift to the right. This inhibits the decomposition of under-cooled austenite, decreases the bainite transformation.

In addition, the dilatometric curves in Fig. 3 show that when the heating temperature is higher than 854 °C at the heating rate of 50 °C/s, the initial microstructure in the sample can be fully

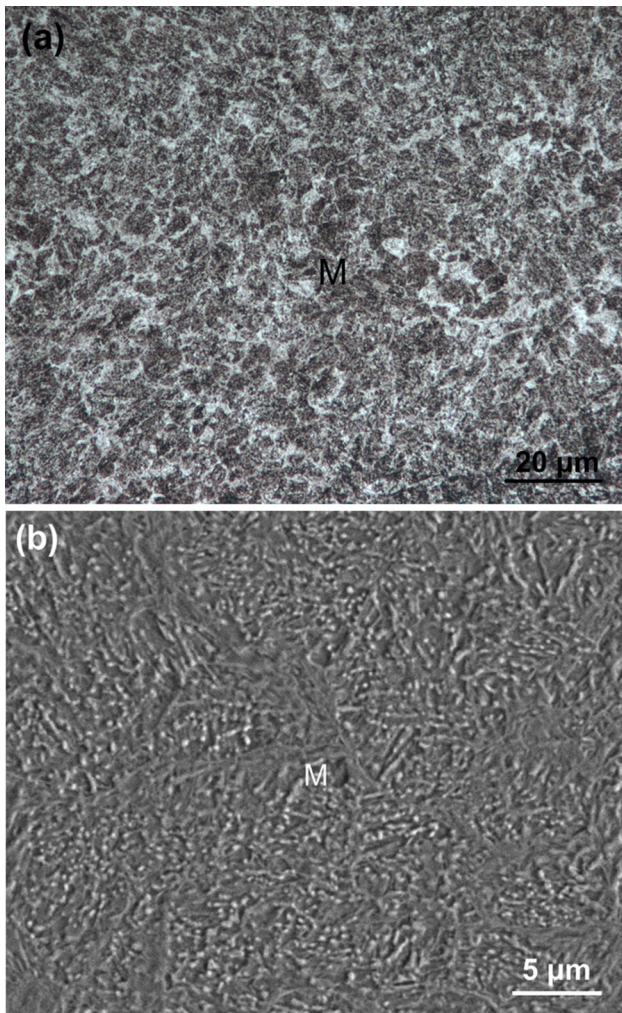


Fig. 12 Microstructure of 55CrMo steel heated at 850 °C for 32 s. (a) Metallographic photograph, (b) SEM micrograph

transformed into austenite during the heating. However, the increasing holding time is also helpful to inhibit ferrite and bainite transformation. Furthermore, the increasing heating temperature helps to achieve a uniform and fine martensite microstructure. Thus, when the heating temperature is not less than 900 °C, only martensite transformation appears in the cooling process at any cooling rates, as shown in Fig. 18(c). It shows that the higher the heating temperature, the smaller the effect of the cooling rate on the phase transformation during the cooling. Further, only martensite phase appears at the cooling rate of 50 °C/s or more.

Microstructure of 55CrMo steel specimen heated at 800–900 °C for 16 s and cooled at the cooling rate of 50–90 °C/s is shown in Fig. 19. Using the same method, the proportion of each phase was estimated as shown in Table 3. With the increasing cooling rate, the volume fraction of martensite increases. As the heating temperature is 800°C or 850°C, and the cooling rate is 70 or 90 °C/s, bainite still can be found in the microstructure, and the morphological feature is not obvious. Figure 19(a), (b), (c), and (d) shows that the microstructure is the mixture of bainite and martensite as the heating temperature is 800 °C or 850 °C. Figure 19(e) and (f) shows that as the heating temperature is 900 °C, the microstructure of specimen

is almost 100% martensite. The selected XRD pattern is shown in Fig. 20. By calculating the volume fraction of retained austenite in the specimen heated at 900 °C and cooled at the different cooling rate, it shows that the cooling rate has no obvious effect on the volume fraction of retained austenite, and the volume fraction of retained austenite is approximately 10.5%.

The results of hardness test (Fig. 21) can be attributed to the observed microstructure shown in Fig. 19. Pearlite, bainite and martensite have been previously described. According to the previously mentioned microstructural constituents, the increasing cooling rate can significantly increase the hardness. The HV value of hardness is depending on the microstructure and increases with the increasing cooling rate (Ref 37). Martensite has the highest hardness, and bainite has an intermediate hardness. As the heating temperature is 900 °C, the hardness value of sample with full martensitic microstructure exceeds 800 HV, it means a high-strength martensitic microstructure is produced in the heat treatment. In summary, as the heating temperature is not less than 900 °C, the cooling rate has a slight effect on the microstructure and microhardness.

However, the heating temperature cannot be too large, as shown in Fig. 22. As the temperature is approximately 1000 °C, and some crack is produced in the cooling process. The grain size of austenite becomes larger due to the high heating temperature, increasing the thermal stress and leading to cracking. Based on the above-mentioned results, the cooling rate should be increased to improve the surface hardness and productivity. However, the risk of cracking and distortion increases with the increasing cooling rate. Figure 22(b) shows that the fracture is characterized by a brittle morphology, and the typical crystal sugar fracture morphology can be observed. Cracks are observed at the high temperature of sample, and these cracks can be attributed to the stresses developed in the steel during the cooling.

3.4 Effect of Heating Temperature on Phase Transformation of 55CrMo Steel

The dilatometric curves of samples heated at the different heating temperature for 16 s and cooled at the cooling rate of 50 °C/s are shown in Fig. 23. According to these dilatometric curves, the martensite start temperature can be attained by the tangent method, it is approximately 314, 276, 273 and 253 °C as the heating temperature is 950, 1000, 1100 and 1200 °C, as shown in Fig. 24. The martensite start temperature decreases with the increasing heating temperature. This is because the heating temperature favors further integration of carbon and alloying elements into the austenite. With the increasing austenitizing uniformity, the stability of undercooled austenite increases, leading to a drop of martensite start temperature. The residual carbides are accompanied by an increase in the carbon content in the matrix, decreasing the martensite start temperature during the cooling. In addition, the content of retained austenite also increases due to the decreasing of martensite start temperature.

Selected XRD patterns of specimen heated as 800–1000 °C are shown in Fig. 25, and the volume fraction of retained austenite in the specimen can be calculated, as shown in Fig. 26. When the heating temperature is low, the alloying elements are not fully incorporated into austenite. In addition, Lambers et al. (Ref 22) also assumed that an incomplete austenitization decreased the content of carbon and alloying

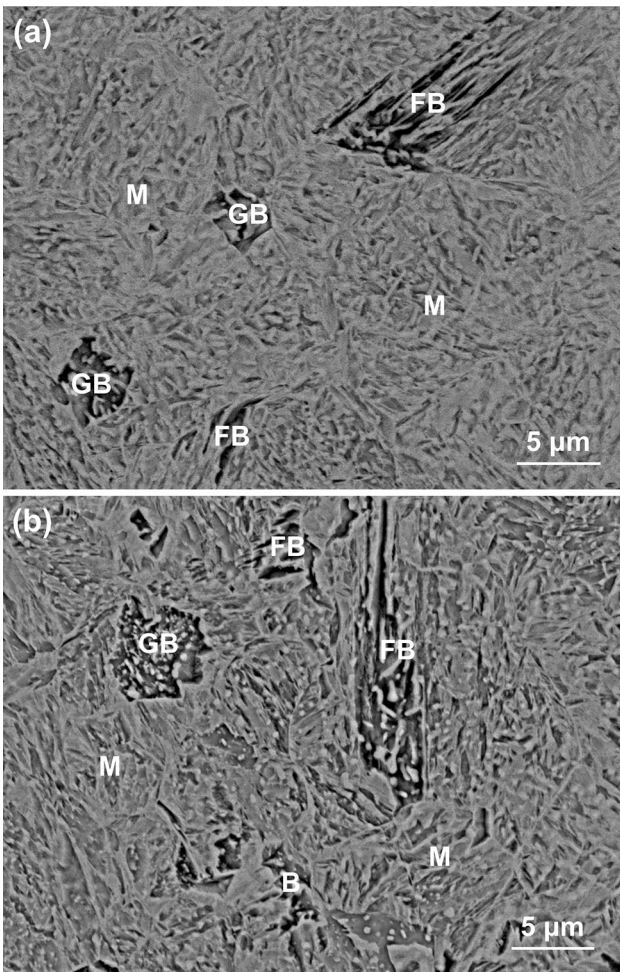


Fig. 13 Bainite microstructure of 55CrMo steel (recorded using the D mode of Nova SEM 450) (F = proeutectoid ferrite, P = perlite, FB = ferrite bainite, GB = granular bainite, M = martensite)

elements in the austenite matrix. Therefore, the retained austenite content is less. When the heating temperature is 850 °C, the initial pearlite transformed into austenite. However, the distribution of the alloy element is uneven in austenite, and there is a rich alloy element zone, increasing the content of austenite. As the heating temperature continues to increase, the austenite is uniform, and the average alloying element content in the austenite decreases, thus decreasing the austenite content at room temperature. When the temperature is 1000 °C, the temperature is too high to dissolve carbide completely, and the content of carbon in austenite increases, increasing the content of retained austenite. Therefore, the results show that with the increasing heating temperature, the volume fraction of retained austenite firstly increases and then decreases. In contrast, when the heating temperature is 1000 °C, the volume fraction of retained austenite increases. As a result, the heating temperature cannot exceed 1000 °C.

Microstructure of specimen heated at the different heating temperature is shown in Fig. 27. It shows that the microstructure is cryptocrystalline martensite as the heating temperature is 950 °C. When the heating temperature is 1000 °C, the microstructure changes from cryptocrystalline martensite to fine needle-like martensite, belonging to the normal microstruc-

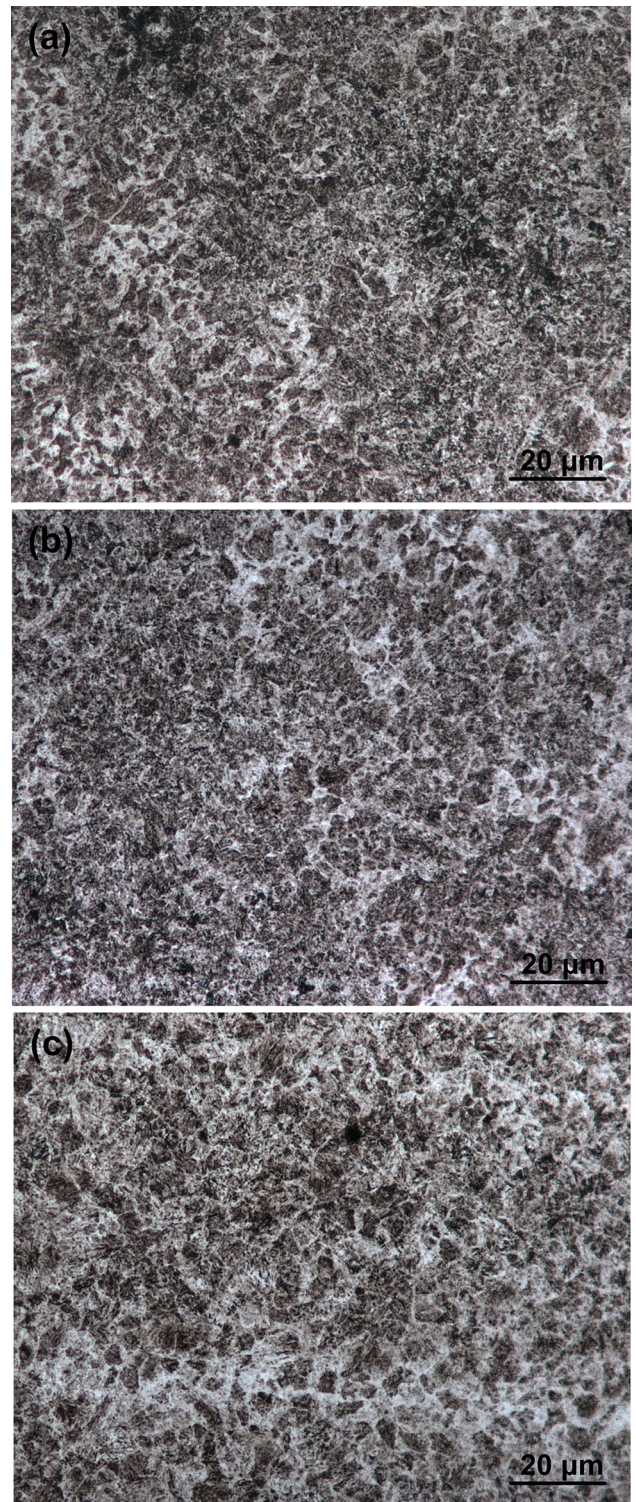


Fig. 14 Microstructure of 55CrMo steel heated at 900 °C for different holding times. (a) 8 s, (b) 16 s, (c) 32 s

ture. When the heating temperature is 1100 °C, the microstructure is lath martensite of hardened medium-carbon steel, and the size of martensite is coarse. With the increasing heating temperature, martensite shows row-like distribution and all with different habitats and tandem nature between the triangular arrangements of the strip, belonging to quenched and over-

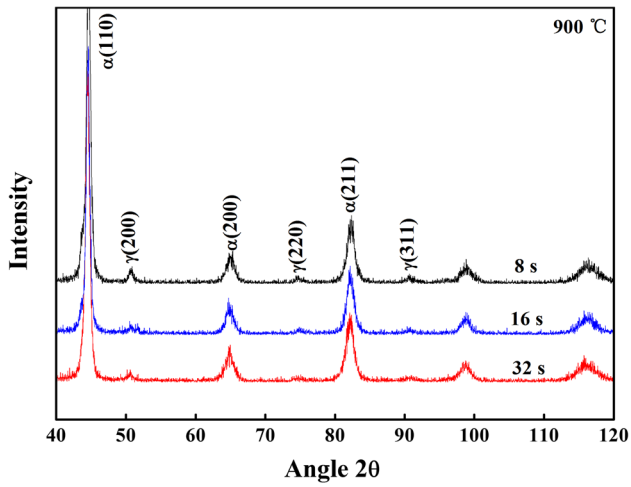


Fig. 15 X-ray diffraction spectra of 55CrMo steel specimens heated at 900 °C for different holding times

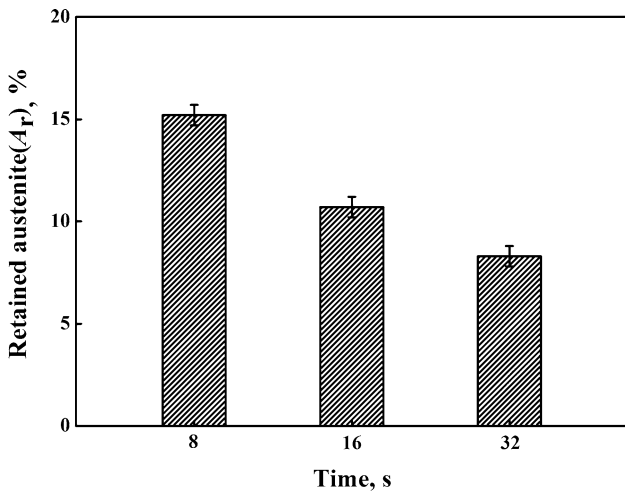


Fig. 16 Volume fraction of retained austenite of 55CrMo steel specimens heated at 900 °C for different holding times

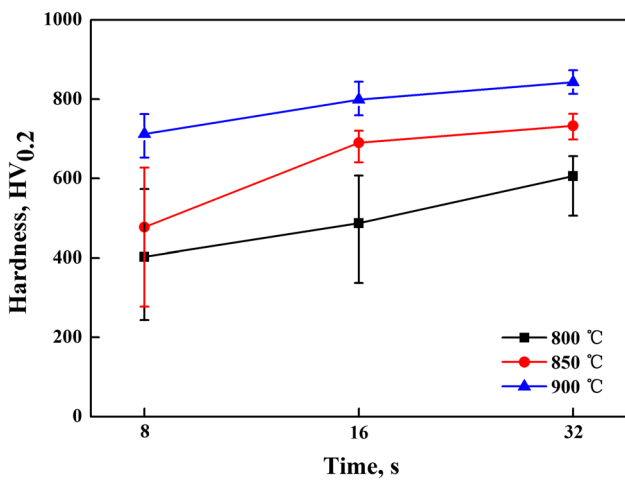
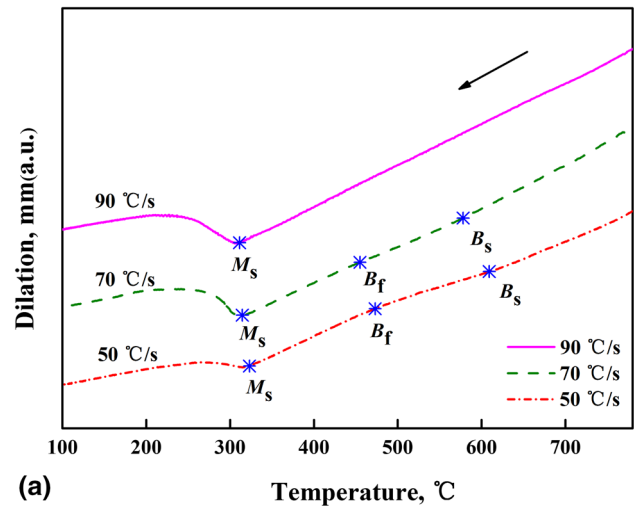
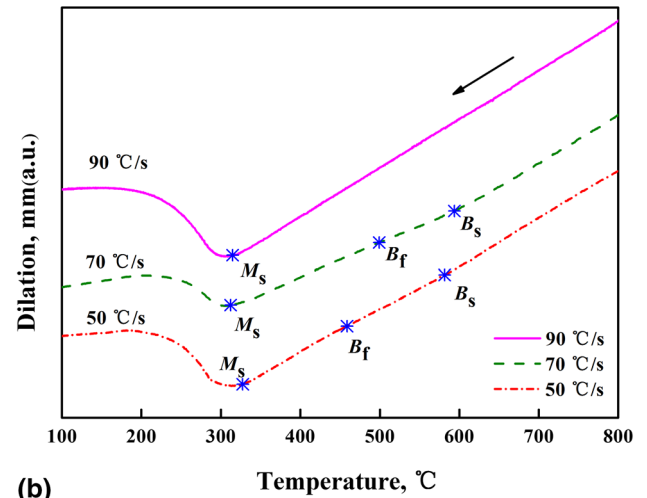


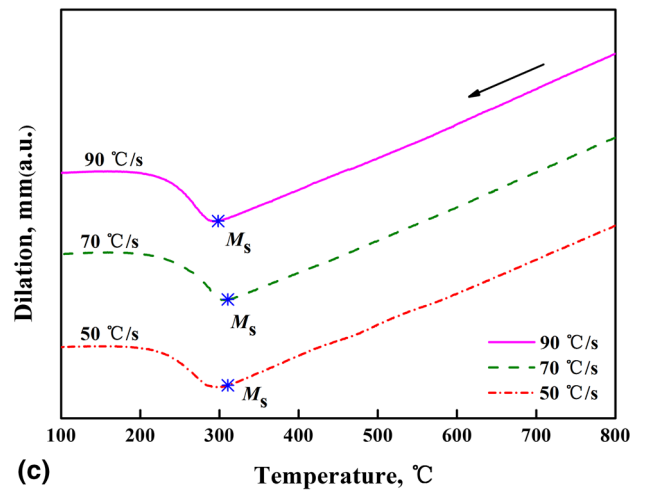
Fig. 17 Microhardness of 55CrMo steel specimens heated at 800 °C, 850 °C and 900 °C for different holding times



(a)



(b)



(c)

Fig. 18 Dilatometric curves of 55CrMo steel at different cooling rates. (a) Heated at 800 °C, (b) Heated at 850 °C, (c) Heated at 900 °C

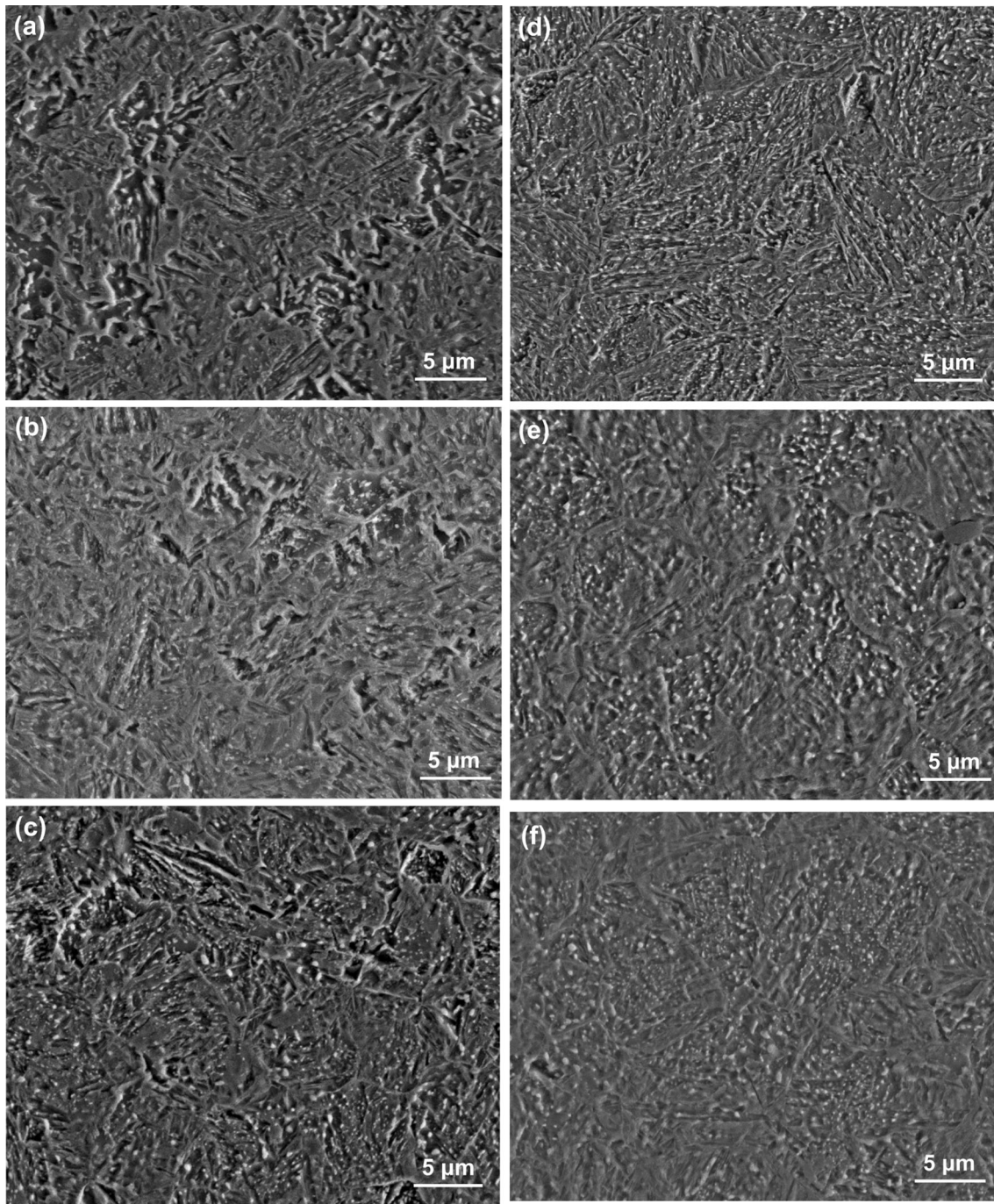


Fig. 19 Microstructure of 55CrMo steel specimens heated at 800-900 °C for 16 s and cooled at the cooling rate of 50-90 °C/s (recorded using Nova SEM 450). (a) 800-70 °C/s, (b) 800-90 °C/s, (c) 850-70 °C/s, (d) 850-90 °C/s, (e) 900-70 °C/s, (f) 900-90 °C/s

heated microstructure. As the heating temperature increases, the grain size growth of austenite occurs, and austenite is transformed into the coarse martensite after quenching. When the heating temperature is 1200 °C, it belongs to a severe overheating microstructure. The grain size is coarse, and martensite is arranged in a polygonal shape. The orientation of the slab bundles in the same grain is not the same. The grain boundary separation and deformation increases, and too much internal stress occurs during quenching, resulting in the internal cracking of sample.

The cryptocrystalline martensite has a good wear resistance and good hardenability. The experimental results also indicate that microstructure of 55CrMo steel heated at 800-1000 °C shows a fine grain size, and the grain size shows an abnormal growth as the heating temperature is above 1000 °C. There are two reasons for this phenomenon. On one hand, in the continuous heating, with the increasing temperature, the diffusion coefficient of carbon increases, and the alloy elements start to diffuse at a certain temperature (Ref 38). The effect of diffusion rate on grain growth is increasingly more significant.

Table 3 Proportions of microstructure of 55CrMo steel at different cooling rates

Content, %	800 °C			850 °C		
	50 °C/s	70 °C/s	90 °C/s	50 °C/s	70 °C/s	90 °C/s
Ferrite + pearlite	8.26%	0	0	2.6%	0	0
Bainite	25.44%	25.6%	13.7%	13.2%	14.3%	1%
Martensite	66.3%	74.4%	86.3%	84.2%	85.7%	99%

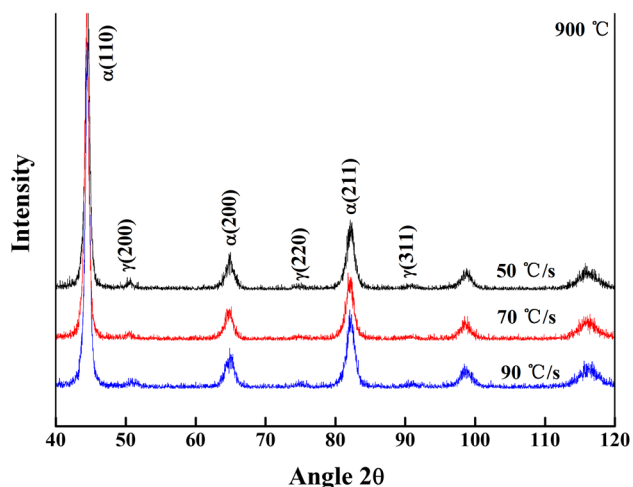


Fig. 20 X-ray diffraction spectra of 55CrMo steel specimens heated at 900 °C and cooled at different cooling rates

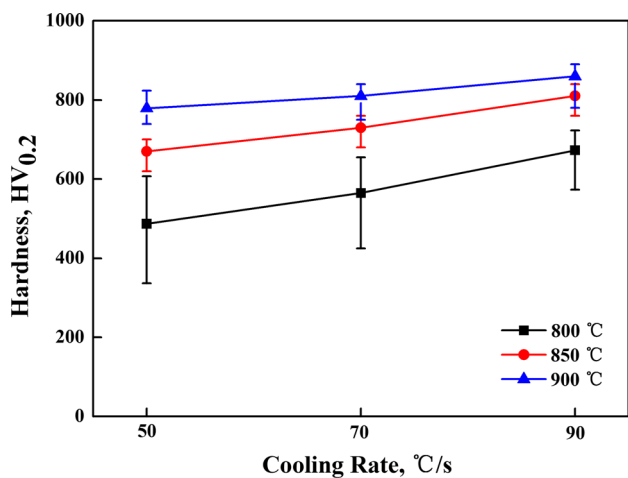


Fig. 21 Microhardness of 55CrMo steel specimens heated at 800, 850 and 900 °C at different cooling rates

According to the grain size theory of Hillert (Ref 39), individual growth of the first grains will prevent the abnormal growth of small grains. On the other hand, the austenitization temperature and time affect the amount of dissolved carbides in the austenite. When the temperature exceeds 1000 °C, chromium, molybdenum, and other elements start to dissolve, and the tendency to suppress the growth of austenite grains decreases. The alloying of austenite is also very full, and the austenite grains start to grow significantly due to carbon diffusion. A larger coarse martensite structure can be obtained

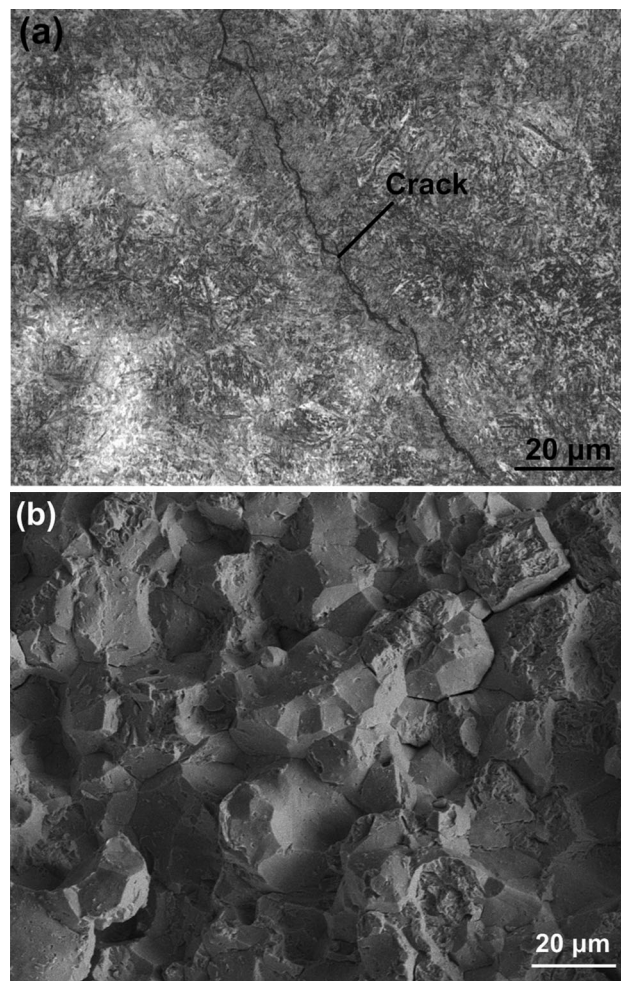


Fig. 22 Microstructure and fracture of 55CrMo steel heated at 1000 °C and cooled at the cooling rate of 70 °C/s. (a) Microstructure, (b) Fracture

after quenching. Thus, the brittleness of steel increases due to the presence of coarse grains.

The alloying elements present in the steel significantly affect the segregation and hardenability (Ref 40). The Cr and Mo elements of 55CrMo steel refine grain, thus improving the hardenability of the material. Thus, the critical point of steel increases, and the rapid growth of grain is hindered. In addition, there are complex carbides, even if the steel heated at 1000 °C for a certain time, the growth of body grains is not significant, and the quenched martensite needles are not too thick. The gray microstructure in the metallographic images is self-tempered martensite. The blurred matrix shows a small hidden needle-like martensite, which is gray, has better mechanical properties

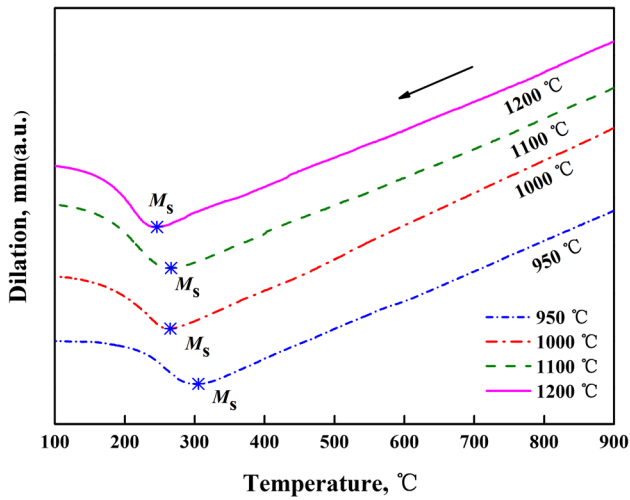


Fig. 23 Dilatometric curves of 55CrMo steel specimens heated at different heating temperatures

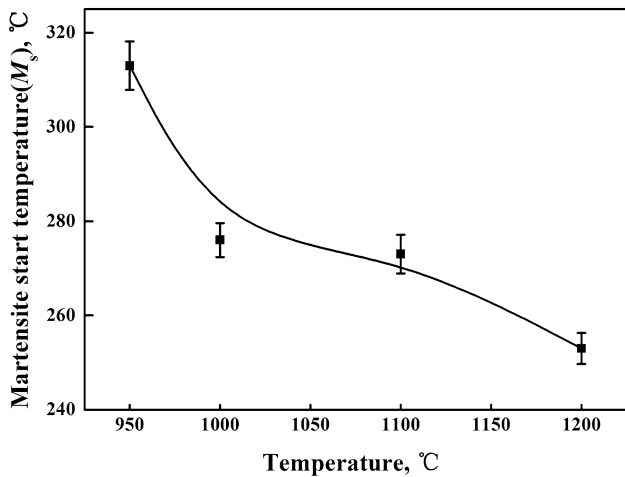


Fig. 24 Relationship between heating temperature and M_s

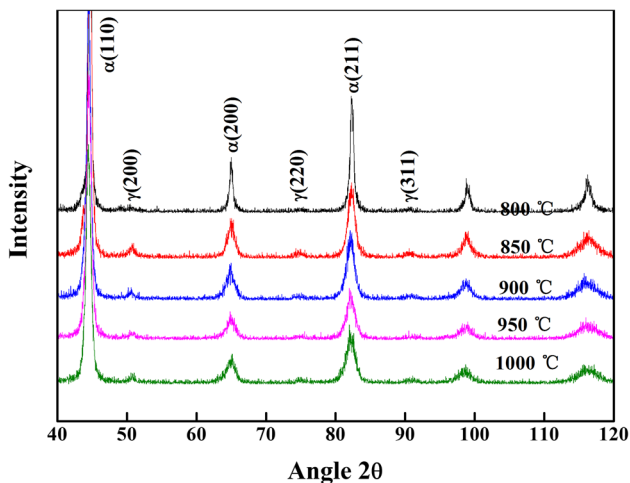


Fig. 25 X-ray diffraction spectra of specimens heated at different heating temperatures

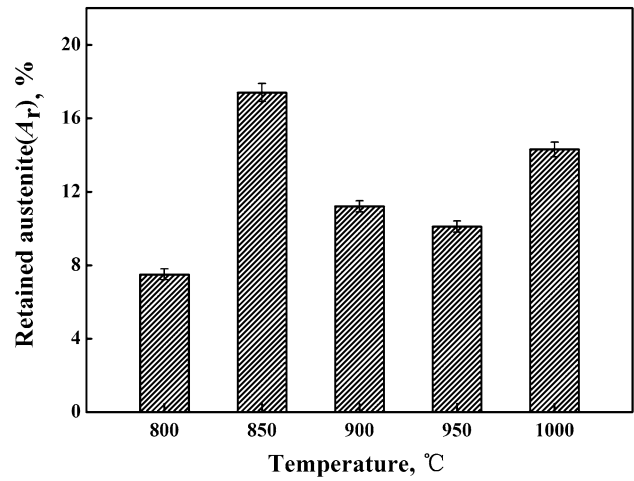


Fig. 26 Volume fraction of retained austenite in the specimen heated at different heating temperatures

and more uniform hardness, and belongs to a normal microstructure. The microhardness is shown in Fig. 28. The carbon enrichment of austenite makes an important contribution to the hardness of martensite during subsequent cooling to room temperature (Ref 41). However, when the heating temperature is 1100 °C, because of the higher heating temperature, although the hardness of steel is still high, a significant growth of austenite grain occurs, the content of retained austenite increases, and the plasticity and toughness of steel decreases accordingly. Therefore, a lower heating temperature will lead to incomplete austenitization of 55CrMo steel, and a higher temperature will affect the final product quality.

The analysis shows that for the induction hardening of 55CrMo steel ball screw, when the moving speed of coils is approximately 240 mm/min, and the gap between the coils and the spraying water circle is approximately 32 mm, the induction heating temperature should be controlled in the range of 900-1000 °C.

4. Conclusions

Heat treatment of 55CrMo steel specimens was performed by the Gleeble-1500D thermal simulator at the different heating temperature, holding time and cooling rate to investigate the effect of induction hardening parameters on the phase transformation, microstructure and microhardness of 55CrMo steel. Some of the conclusions are as follows:

1. Induction hardening is different from conventional quenching, which is favorable for the microstructure refinement of 55CrMo steel and beneficial to obtain the cryptocrystalline martensite with a better performance.
2. At a heating rate of 50 °C/s, when the heating temperature is 800 °C and 850 °C, the austenitizing temperature is too low. The austenitization is not enough, and bainite microstructure appears during the cooling.
3. At a certain heating rate, the increasing heating temperature and holding time can promote the original microstructure dissolution, and increase the stability of undercooled austenite and the content of martensite.

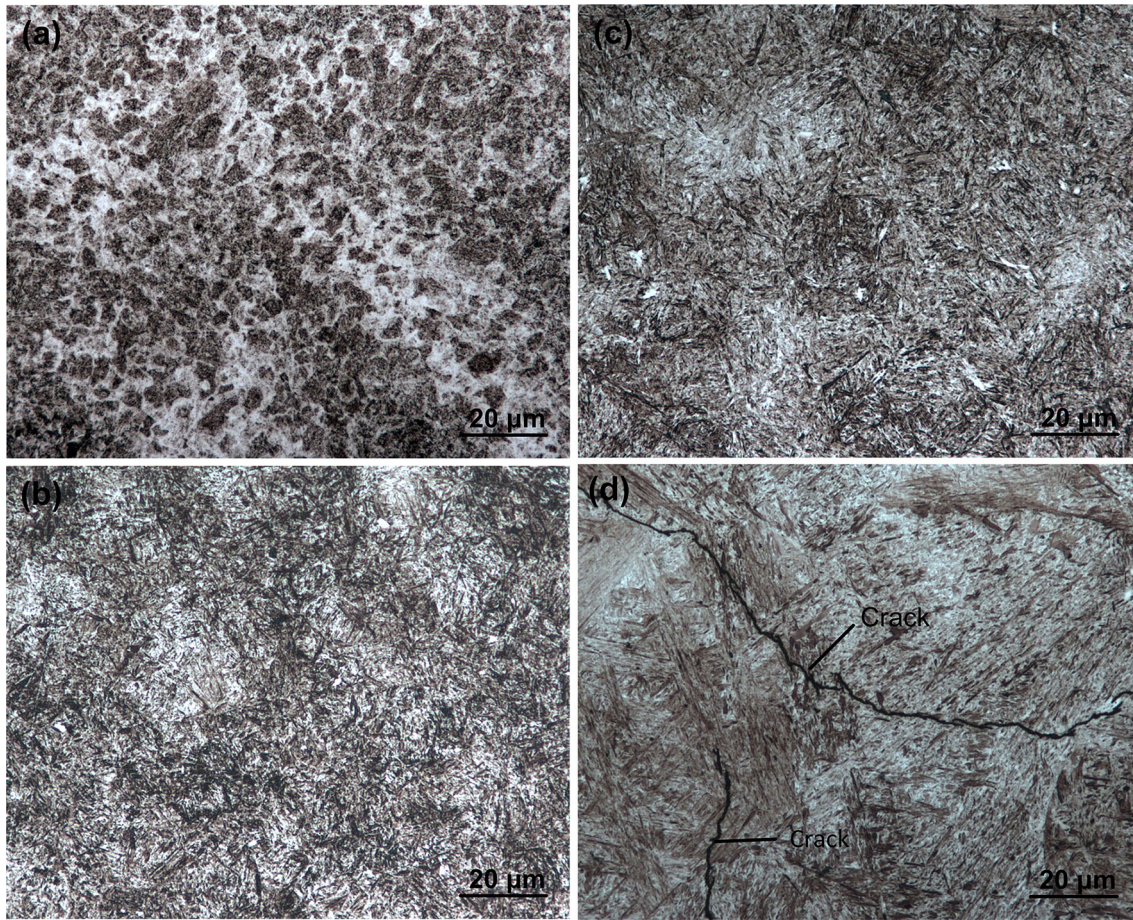


Fig. 27 Microstructure of specimen heated at different heating temperatures. (a) 950 °C, (b) 1000 °C, (c) 1100 °C, (d) 1200 °C

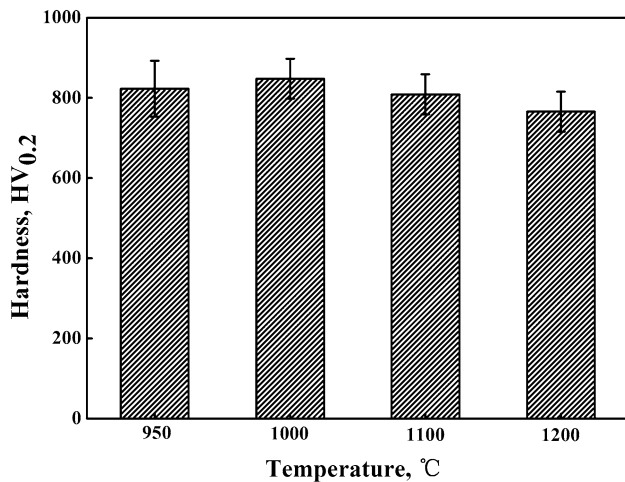


Fig. 28 Microhardness of specimens heated at different heating temperatures

- The results of retained austenite test show that the volume fraction of retained austenite is less as the heating temperature is 900 or 950 °C. The heating temperature could not exceed 1000 °C.
- High temperature leads to coarse grains and results in crack. The induction heating temperature of 55CrMo steel should be controlled in the temperature range of 900-1000 °C.

Acknowledgments

This work was financially supported by the National Natural Science Foundation of China (51575324), and the Science and Technology Development Program of Shandong (2014GGX 103024).

References

- D. Zapata, J. Jaramillo, and A. Toro, Rolling Contact and Adhesive Wear of Bainitic and Pearlitic Steels in Low Load Regime, *Wear*, 2011, **271**(1), p 393–399
- S. Gündüz, R. Kaçar, and H.Ş. Soykan, Wear Behaviour of Forging Steels with Different Microstructure During Dry Sliding, *Tribol. Int.*, 2008, **41**(5), p 348–355
- Y.H. Wu, Quality Control of Surface Inductive Quenching for Ball Screw, *Heat Treat. Met.*, 2011, **36**(1), p 120–121 (In Chinese)
- Y. Yan, Y.H. Gai, B.M. Li, Q.X. Dong, and M.S. Li, Quality Analysis of Gcr15 Steel Ball Screw After Quenched by Tilted Inductor, *Heat Treat. Technol. Equip.*, 2014, **35**(1), p 17–20 (In Chinese)
- J.L. Cunningham, D.J. Medlin, and G. Krauss, Effects of Induction Hardening and Prior Cold Work on a Microalloyed Medium Carbon Steel, *J. Mater. Eng. Perform.*, 1999, **8**(4), p 401–408
- C.R.F. Azevedo and J.B. Neto, Failure Analysis of Forged and Induction Hardened Steel Cold Work Rolls, *Eng. Fail. Anal.*, 2004, **11**(6), p 951–966
- S.T. Ahn, D.S. Kim, and W.J. Nam, Microstructural Evolution and Mechanical Properties of Low Alloy Steel Tempered by Induction Heating, *J. Mater. Process. Technol.*, 2005, **160**(1), p 54–58
- M.H. Kim, K.Y. Rhee, Y.N. Paik, J.S. Hong, and Y.S. Ham, Experimental Investigation on the Mechanical Behavior of High-

- Frequency Induction-Hardened Mild Carbon, SPS5 Steel, *Mater. Sci. Eng. A*, 2008, **485**(1–2), p 31–38
9. H. Kristoffersen and P. Vomacka, Influence of Process Parameters for Induction Hardening on Residual Stresses, *Mater. Des.*, 2001, **22**(22), p 637–644
 10. C. Revilla, B. López, and J.M. Rodríguez-Ibabe, Carbide Size Refinement by Controlling the Heating Rate During Induction Tempering in a Low Alloy Steel, *Mate. Des.*, 2014, **62**(62), p 296–304
 11. X. Zhu, T. Zhang, D. Marchant, and V. Morris, The Structure and Properties of NiAl Formed by SHS Using Induction Heating, *Mater. Sci. Eng. A*, 2011, **528**(3), p 1251–1260
 12. A. Danon, C. Servant, A. Alamo, and J.C. Brachet, Heterogeneous Austenite Grain Growth in 9Cr Martensitic Steels: Influence of the Heating Rate and the Austenitization Temperature, *Mater. Sci. Eng. A*, 2003, **348**(1–2), p 122–132
 13. M.C. Kayacan and O. Çolak, A Fuzzy Approach for Induction Hardening Parameters Selection, *Mate. Des.*, 2004, **25**(2), p 155–161
 14. A. Zabeti and S.H.M. Azghandi, Simulation of Induction Tempering Process of Carbon Steel Using Finite Element Method, *Mate. Des.*, 2012, **36**, p 415–420
 15. B.J. Yang, A. Hattiangadi, W.Z. Li, G.F. Zhou, and T.E. McGreevy, Simulation of Steel Microstructure Evolution During Induction Heating, *Mater. Sci. Eng. A*, 2010, **527**(12), p 2978–2984
 16. H. Li, G. Zhao, and L. He, Finite Element Method Based Simulation of Stress–Strain Field in the Quenching Process, *Mater. Sci. Eng. A*, 2008, **478**(1–2), p 276–290
 17. J. Yuan, J. Kang, Y. Rong, and R.D. Sisson, Jr., FEM Modeling of Induction Hardening Processes in Steel, *J. Mater. Eng. Perform.*, 2003, **12**(5), p 589–596
 18. G.Y. Zhang, X.Q. Xi, and W.Y. Zhang, Optimization of Induction Quenching Process Parameters and Prediction of Microstructure and Hardness Distribution for S45C Steel Shaft, *Trans. Mater. Heat Treat.*, 2013, **34**(6), p 174–179
 19. D. Hömberg, T. Petzold, and E. Rocca, Analysis and Simulations of Multifrequency Induction Hardening, *Nonlinear Anal. Real.*, 2015, **22**(1), p 84–97
 20. J. Barglik, A. Smalcerz, R. Przylucki, and I. Doležel, 3D Modeling of Induction Hardening of Gear Wheels, *J. Comput. Appl. Math.*, 2014, **270**(1), p 231–240
 21. H. Li, L. He, K. Gai, R. Jiang, C. Zhang, and M. Li, Numerical Simulation and Experimental Investigation on the Induction Hardening of a Ball Screw, *Mate. Des.*, 2015, **87**, p 863–876
 22. H.G. Lambers, S. Tschumak, H.J. Maier, and D. Canadinc, Role of Austenitization and Pre-deformation on the Kinetics of the Isothermal Bainitic Transformation, *Metall. Mater. Trans. A*, 2009, **40**(6), p 1355–1366
 23. K.D. Clarke, C.J. Van Tyne, C.J. Vigil, and R.E. Hackenberg, Induction Hardening 5150 Steel: Effects of Initial Microstructure and Heating Rate, *J. Mater. Eng. Perform.*, 2011, **20**(2), p 161–168
 24. H. Li, K. Gai, L. He, C. Zhang, H. Cui, and M. Li, Non-isothermal Phase-Transformation Kinetics Model for Evaluating the Austenitization of 55CrMo Steel Based on Johnson–Mehl–Avrami Equation, *Mate. Des.*, 2016, **92**, p 731–741
 25. C. Lesch, P. Álvarez, W. Bleck, and J.G. Sevillano, Rapid Transformation Annealing: A Novel Method for Grain Refinement of Cold-Rolled Low-Carbon Steels, *Metall. Mater. Trans. A*, 2007, **38**(9), p 1882–1890
 26. C.G.D. Andrés, F.G. Caballero, C. Capdevila, and L.F. Álvarez, Application of Dilatometric Analysis to the Study of Solid–Solid Phase Transformations in Steels, *Mater. Charact.*, 2002, **48**(1), p 101–111
 27. B.K. Jha, R. Avtar, and V. Dwivedi, Structure-Property Correlation in Low Carbon Low Alloy High Strength Wire Rods/Wires Containing Retained Austenite, *Trans. Ind. Inst. Met.*, 1996, **49**(3), p 133–142
 28. B. Pawłowski, P. Bała, and R. Dziurka, Improper Interpretation of Dilatometric Data for Cooling Transformation in Steels, *Arch. Metall. Mater.*, 2014, **59**(3), p 1159–1161
 29. T.A. Kop, J. Sietsma, and S.V.D. Zwaag, Dilatometric Analysis of Phase Transformations in Hypo-Eutectoid Steels, *J. Mater. Sci.*, 2001, **36**(2), p 519–526
 30. M.D. Geib, D.K. Matlock, and G. Krauss, The Effect of Intercritical Annealing Temperature on the Structure of Niobium Microalloyed Dualphase Steel, *Metall. Mater. Trans. A*, 1980, **11**(10), p 1683–1689
 31. M. Kang, M. Zhu, and M. Zhang, Mechanism of bainite nucleation in steel, iron and copper alloys, *J. Mater. Sci. Technol.*, 2005, **21**(4), p 437–444
 32. J.J. Li and G. Andrew, Effects of Austenitization and Cooling Rates on the Microstructure in a Hyper-Eutectoid Steel, *Acta Metall. Sin.*, 2013, **49**(5), p 583 (in Chinese)
 33. S. Zaeferrer, J. Ohlert, and W. Bleck, A Study of Microstructure, Transformation Mechanisms and Correlation Between Microstructure and Mechanical Properties of a Low Alloyed TRIP Steel, *Acta Mater.*, 2004, **52**(9), p 2765–2778
 34. M.X. Zhang and P.M. Kelly, Accurate Orientation Relationship Between Ferrite and Austenite in Low Carbon Martensite and Granular Bainite, *Scr. Mater.*, 2002, **47**(11), p 749–755
 35. Z.C. Liu and H.P. Ren, *Diffusion Phase Transformation of Supercooled Austenite*, Science Press, Beijing, 2007 (in Chinese)
 36. V. Massardier, A. Ngansop, D. Fabrègue, and J. Merlin, Identification of the Parameters Controlling the Grain Refinement of Ultra-Rapidly Annealed Low Carbon Al-Killed Steels, *Mater. Sci. Eng. A*, 2010, **527**(21–22), p 5654–5663
 37. H. Li, G. Zhao, S. Niu, and C. Huang, FEM Simulation of Quenching Process and Experimental Verification of Simulation Results, *Mater. Sci. Eng. A*, 2007, **452–453**(24), p 705–714
 38. T. Lolla, G. Cola, B. Narayanan, B. Alexandrov, and S.S. Babu, Development of Rapid Heating and Cooling (Flash Processing) Process to Produce Advanced High Strength Steel Microstructures, *Mater. Sci. Technol.*, 2011, **27**(5), p 863–875
 39. M. Hillert, On the Theory of Normal and Abnormal Grain Growth, *Acta Metall.*, 1965, **13**(3), p 227–238
 40. M. Yamada, Effects of Alloying Elements on the Hardenability, Toughness and the Resistance of Stress Corrosion Cracking in 1 to 3 mass% Cr Low Alloy Steel, *ISIJ Int.*, 2014, **54**(1), p 240–247
 41. W.W. Bose-Filho, A.L.M. Carvalho, and M. Strangwood, Effects of Alloying Elements on the Microstructure and Inclusion Formation in HSLA Multipass Welds, *Mater. Char.*, 2007, **58**(1), p 29–39